Experimental Study of the Micelle-to-Vesicle Transition

J. Oberdisse,[†] O. Regev,[‡] and G. Porte*,[†]

Groupe de Dynamique des Phases Condensées, UMR 5581 du CNRS, Université Montpellier II C.C. 26, Place Eugène Bataillon, 34095 Montpellier Cedex 05, France, and Department of Chemical Engineering, Ben-Gurion University, Box 653, 84105 Beer-Sheva, Israel

Received: July 23, 1997; In Final Form: November 10, 1997

A study of the transition from spherical micelles to wormlike micelles to vesicles in an amphiphilic system with strong electrostatic interactions is presented. We combine small-angle neutron scattering (SANS) and cryo-transmission electron microscopy (cryo-TEM) for a characterization of supramolecular aggregates at low concentration as a function of cosurfactant-to-surfactant ratio. Micellar radii and lengths are monitored, and the phase boundaries are determined. At higher concentration, evidence for an onion-type structure is found.

I. Introduction

In past years several studies on spontaneously forming vesicles in amphiphilic systems have been reported.[1−7] In most of these systems a transition from micelles—first spherical, then wormlike—to vesicles is observed, and it is triggered by a change in aggregate composition.

In a recent article, we have investigated the effect of an ionic surfactant on a reference system of nonionic surfactant and cosurfactant in water.[8a] In both the neutral and the doped system, we found the same standard sequence of aggregate morphologies, governed by the cosurfactant-to-surfactant ratio: spherical micelles, wormlike micelles, bilayers. However, in the ionic system bilayers are generally curved and—at high dilution—unilamellar vesicles are formed. In a second publication we could show that the electrostatic double layer has an decisive influence on the radius of the vesicles.[8b]

In this article, we focus on the micelle-to-vesicle transition in the presence of strong electrostatic interactions. A cosurfactant-induced micelle-to-vesicle transition is studied by a combination of direct imaging and SANS and conductivity measurements.

II. Experimental Section

The System. Triton X-100 is the nonionic surfactant, and octanol is the neutral cosurfactant. The relative quantity is expressed by the cosurfactant-to-surfactant ratio Ω: $\Omega = [\text{Oct}]/[\text{TX-100}]$ in mass. The ionic additive used is cetylpyridinium chloride (CPCl). Its relative amount Γ is defined in weight fraction as: $\Gamma = [\text{CPCl}]/([\text{CPCl}] + [\text{TX-100}] + [\text{Oct}])$. The total concentration Φ of amphiphile in weight fraction is $\Phi = ([\text{CPCl}] + [\text{TX-100}] + [\text{Oct}])/[\text{total sample mass}]$.

Triton X-100 is purchased from Labosi (technical grade) and used with no further purification. This surfactant, which is of great industrial interest, cannot be considered as a pure chemical compound due to its polydispersity in the polyoxyethylene chain length distribution, which is averaged to 9.5. To preserve mutual consistency between different samples, all solutions were made from the same TX-100 batch. TX-100 is deionized in a 5% aqueous solution. Octanol is purchased from Carlo Erba (analytical grade) and used as received. Water is first doubly distilled and then further deionized using standard ion-exchange resins down to a conductivity of less than10^{-1} μSiemens/cm. The ionic surfactant used as the additive is cetylpyridinium chloride (CPCl) purchased from Fluka (purum grade) and purified along several recrystallizations from ethanol−acetone mixtures.

Cryo-Transmission Electron Microscopy. Direct information on supramolecular structures is obtained by the low-temperature or cryogenic transmission electron microscopy technique (cryo-TEM). The samples are prepared in a controlled environment vitrification chamber[9] at room temperature, and the relative humidity is kept at about 100% to prevent drying of the sample. A 5-μL drop of the solution is put on a TEM grid supported by carbon-coated perforated polymer film.[10] The drop is gently blotted by a filter paper, creating a thin film of the liquid over the grid, which is, immediately after the blotting, vitrified in liquid ethane at its freezing temperature. It is then transferred under liquid nitrogen environment to a cold stage (model 626, Gatan, Inc., Warrendale, PA) and into the electron microscope (JEOL 1200EXII) operated at 100 kV in conventional TEM mode. The working temperature is below 105 K, and the images are recorded on SO-163 film.

Small-Angle Neutron Scattering. All neutron scattering data are collected on-line PACE at the Laboratoire Leon Brillouin in Saclay. For all samples, D_2O is used as the aqueous solvent for obvious contrast reasons.[11] All spectra have been normalized using the incoherent scattering of H_2O, and the resulting intensities are in inverse centimeters. Two wavelengths and sample−detector distances have been used ($\lambda = 6.08$ Å at $d = 200$ cm; $\lambda = 9.48$ Å at $d = 458$ cm) in order to cover the complete q-range: $q = 4.3 \times 10^{-3}$ Å^{-1} to 0.16 Å^{-1}.

Conductivity. A commercially available Microprocessor Conductivity Meter, LF 537 (WTW, Weilheim, Germany) is used. All measurements have been done at $T = 20$ °C and at a frequency of 1000 Hz.

III. Results

Dilute Part of the Phase Diagram. In Figure 1, we show the dilute part of the phase diagram. The horizontal axis

* To whom correspondence should be addressed.
[†] Université Montpellier II C.C. 26.
[‡] Ben-Gurion University.

S1089-5647(97)02390-0 CCC: $15.00
Published on Web 01/22/1998

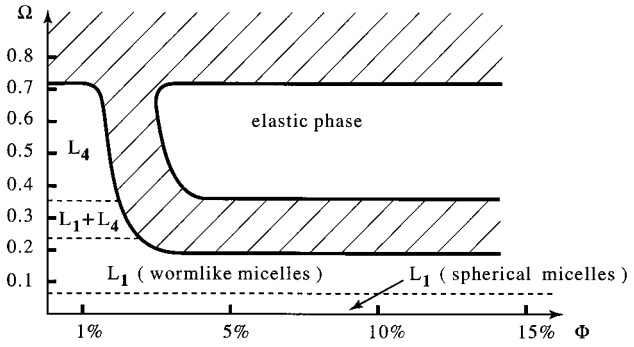

Figure 1. Dilute part of phase diagram of the system TX-100/octanol/CPCl/H_2O at fixed relative amount of charge $\Gamma = 3.55\%$ ($T = 20$ °C).

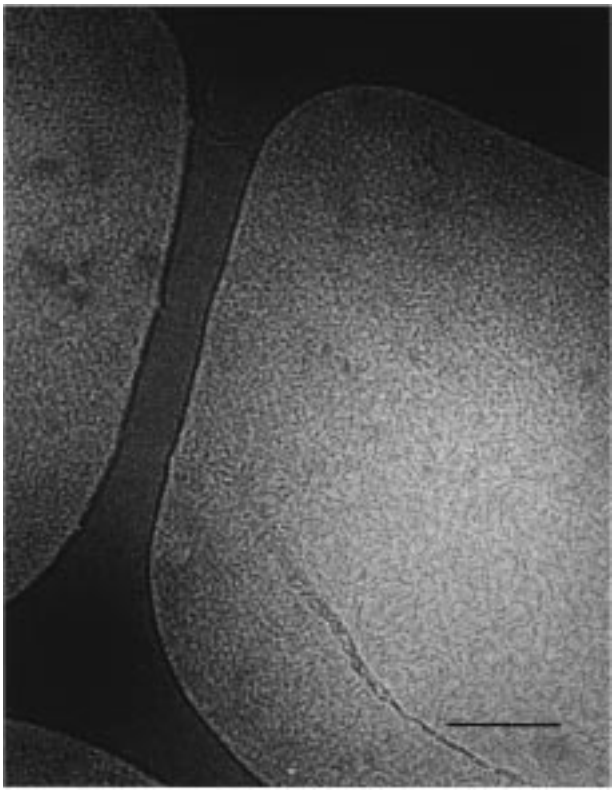

Figure 2. Cryo-TEM image at $\Omega = 0.20$, $\Phi = 1.0\%$, bar = 1000 Å.

corresponds to the total amphiphile concentration Φ and the vertical axis to the cosurfactant-to-surfactant ratio Ω. This section of the total phase diagram is taken at fixed temperature ($T = 20$ °C), atmospheric pressure, and fixed relative amount of CPCl ($\Gamma = 3.55\%$). In the high-Ω range (between 0.4 and 0.8), where bilayers are stable, we find two distinct phases: at moderate dilution ($\Phi > 3$ or 4%), "onion"-like multilayered objects are stable, making the phase very viscoelastic; at high dilution ($\Phi < 2$ or 3% typically) a very fluid dispersion of vesicles is found which we denote L_4: it is continuously connected to the regular micellar phase L_1 at lower Ω. In this article, we will focus on the phase transition between the micellar to the vesicular phase at low concentration.

Cryo-Transmission Electron Microscopy. The effects of cosurfactant-to-surfactant ratio (Ω) and concentration (Φ) were elucidated by cryo-TEM measurements.

Effect of Added Cosurfactant. At constant concentration ($\Phi = 1.0\%$) a transition from elongated to spherical aggregates is detected in the micrographs when the cosurfactant-to-surfactant ratio is increased from 0.20 (Figure 2) to 0.50 (Figure 3). The spherical aggregates are 50−60 Å in diameter. The elongated

Figure 3. Cryo-TEM image at $\Omega = 0.50$, $\Phi = 1.0\%$, bar = 1000 Å.

aggregates look rather flexible. Their average length is about 300−500 Å.

Both the spherical and the elongated aggregates are concentrated near the polymer support (the dark straps in the figures). The vitrified film is thicker at this point due to its meniscus,[12] and hence a crowding of the aggregates is induced. Another indication for this phenomena is the darker film near the polymer support (indicating thicker film) in comparison with the film far from the support. It is therefore possible to observe isolated elongated aggregates only in the brighter part of Figure 3, far from the polymer support, since near it the elongated aggregates overlap.

We will show in the SANS section that the aggregates in the ($\Phi = 1.0\%$, $\Omega = 0.50$, $\Gamma = 3.55\%$)-sample are microvesicles with a diameter of 160−200 Å. We explain the discrepancy in the globular aggregates' diameter between SANS and cryo-TEM results in terms of contrast: The headgroup of the TX-100 surfactant is a hydrophilic chain consisting of about 10 ethoxy groups. These groups are invisible for the electron beam of the microscope since there is very little difference in electron density with the water.[13,14] However, they are detectable by SANS, as the typical value for the contrast of a hydrogenated−deuterated interface is 6×10^{10} cm^{-2}.[11] This difference in contrast is sufficient to explain the discrepancy between SANS data and cryo-TEM. As the observed object in the micrograph is just a dark dot, the inner empty space of the microvesicle is below the microscope resolution and therefore not detected.

Effect of Concentration. With increasing concentration from $\Phi = 1.0\%$ to 5.0%, keeping the cosurfactant-to-surfactant ratio constant at $\Omega = 0.50$, one moves to the isotropic elastic phase.

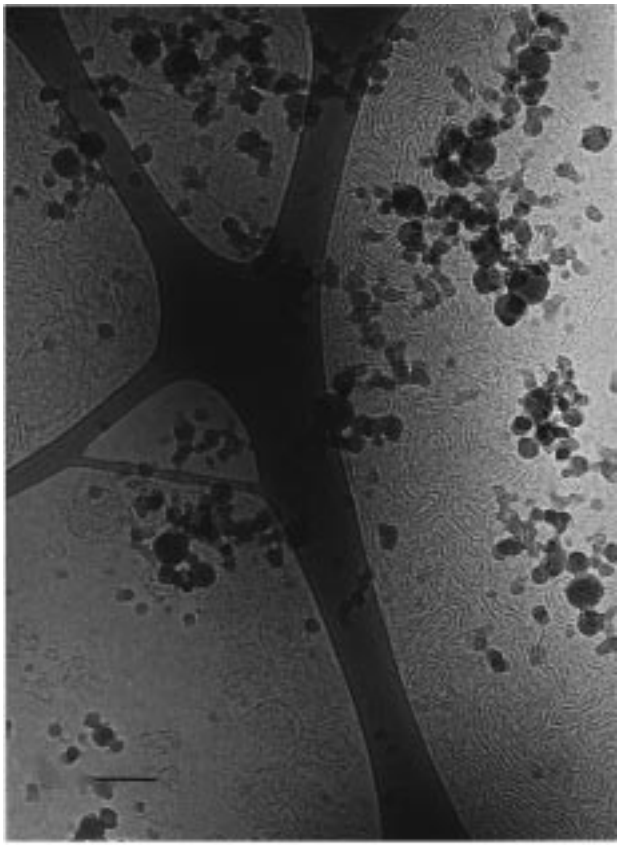

Figure 4. Cryo-TEM image at $\Omega = 0.50$, $\Phi = 5.0\%$, bar = 1000 Å.

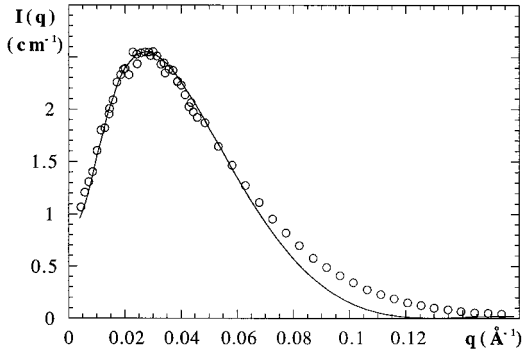

Figure 5. Intensity as a function of wave vector q from SANS (circles; $\Phi = 1.0\%$, $\Omega = 0.0$, $\Gamma = 3.55\%$) compared to a model calculation (see text) of electrostatically interacting spherical micelles (charge $Q = 5 \pm 2$, radius $R_s = 35 \pm 1$ Å).

The microvesicles at $\Phi = 1.0\%$ (Figure 3) turn onionlike at $\Phi = 5.0\%$ (Figure 4).

The onions' diameter is on the order of few thousands angstrom and their d spacing is about 100−150 Å. This aggregation form has already been observed both by freeze-fracture[1] and cryo-TEM[7a] techniques. Recently, Auguste et al. and Dubois et al. published a study of large onions in a charged system (refs 15, 16; see also ref 17). This does not seem to be only a transient texture; it replaces the lamellar phase in well-defined regions of the phase diagram.

The lamellar pattern displayed in many regions of Figure 4 indicates and explains the smectic type of scattering pattern (Figure 9 in ref 8a). The d spacing reported from scattering for $\Phi = 5.0\%$ is about 600 Å (Figure 10 in ref 8a). Our much smaller d spacing (100−150 Å) observed in the micrographs could be explained by a concentration gradient in the sample that might be a result of crowding of objects in the formed film

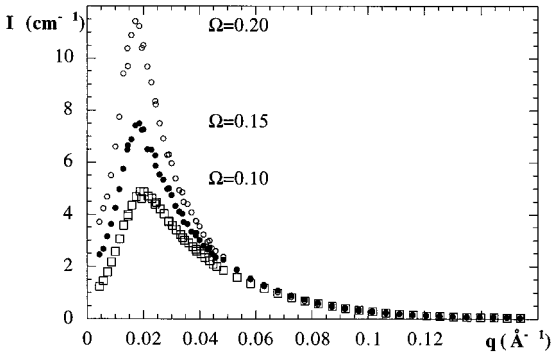

Figure 6. Intensity as a function of wave vector q from SANS for different cosurfactant-to-surfactant ratios Ω (at $\Phi = 1.0\%$, $\Gamma = 3.55\%$): $\Omega = 0.10$, $\Omega = 0.15$, $\Omega = 0.20$.

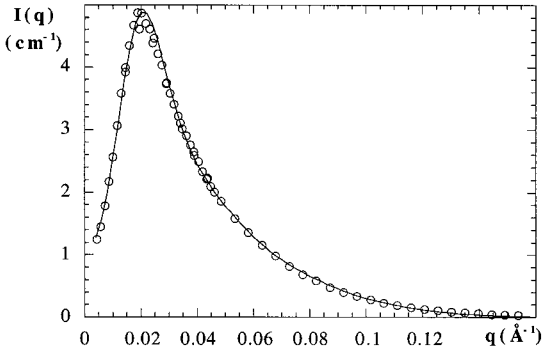

Figure 7. Intensity as a function of wave vector q from SANS (circles; $\Phi = 1.0\%$, $\Omega = 0.10$, $\Gamma = 3.55\%$) compared to a model calculation (see text) of electrostatically interacting cylindrical micelles (charge $Q = 12 \pm 2$, radius $R_c = 23 \pm 1$ Å, length $L = 200 \pm 5$ Å).

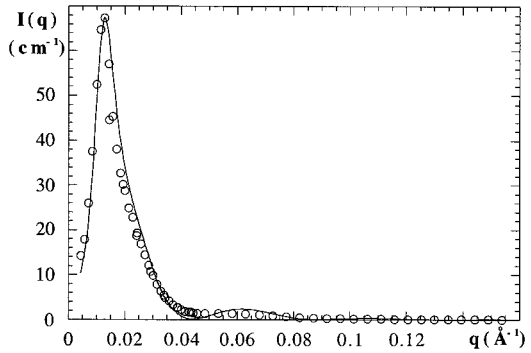

Figure 8. Intensity as a function of wave vector q from SANS (circles; $\Phi = 1.0\%$, $\Omega = 0.60$, $\Gamma = 3.55\%$) compared to a model calculation (see text) of electrostatically interacting unilamellar vesicles (charge $Q = 32 \pm 2$, mean radius $R_v = 70 \pm 1$ Å, bilayer thickness $\delta = 33 \pm 1$ Å).

due to the film's meniscus discussed earlier. This phenomenon is well-documented in several previous papers.[7c,18]

Small-Angle Neutron Scattering (SANS). We interpret the spectra obtained by SANS by fitting form and structure factors. The changes in form and size of the supramolecular aggregates result in a number of qualitative changes that allow for an unambiguous identification of the aggregate transformations: the growth from spherical micelles to cylindrical micelles and the transformation to vesicles is accompanied by a significant increase of the aggregation number, which in turn leads to an increase of the scattered intensity (in cm^{-1}). As we keep the concentration fixed at $\Phi = 1.0\%$, bigger objects are on the average further away, and thus the peak of the structure factor—due to strong electrostatic interactions—shifts to lower q-values.

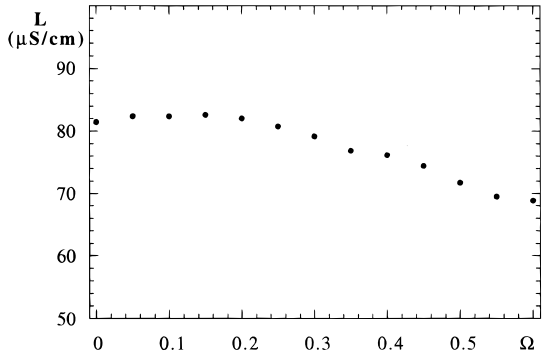

Figure 9. Conductivity as a function of cosurfactant-to-surfactant ratio Ω along the micelle-to-vesicle transition.

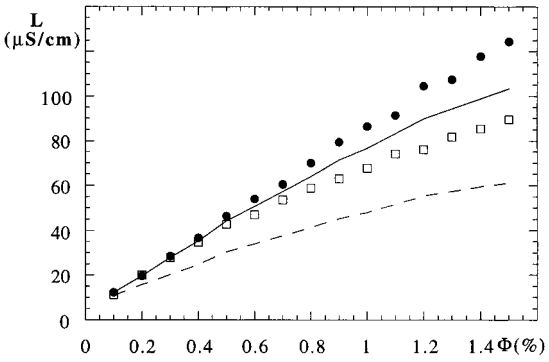

Figure 10. Conductivity as a function of concentration Φ for the micellar phase (Ω = 0.00; full circles) and the vesicular phase (Ω = 0.60; empty squares). The full line is a prediction of the vesicle conductivity according to eq 5; the dotted line is the prediction of the second model.

For the quantitative analysis of the spectra, the form factors of spheres, cylinders, and vesicles are given in the Appendix. To take the electrostatic interactions between charged supramolecular aggregates into account, we use the structure factor $S(q)$ calculated according to the Hayter−Penfold procedure, with the renormalization of Hansen and Hayter, that is, the so-called renormalized mean spherical approximation (RMSA) structure factor.[19]

The general equation for the scattered intensity of identical homogeneous objects with only position correlation is given by

$$I(q) = \frac{N}{V}[|\langle F(q)\rangle|^2 S(q) + \langle |F(q)|^2\rangle - |\langle F(q)\rangle|^2] \qquad (1)$$

where N is the number of objects in a volume V and $F(q)$ is the spatial Fourier transform of the contrast. The brackets $\langle\ \rangle$ indicate an average over all orientations of objects. For a monodisperse distribution of identical spherical objects the scattered intensity can be written

$$I(q) = \frac{N}{V} S(q)\langle |F(q)|^2\rangle \qquad (2)$$

as $\langle |F(q)|^2\rangle = |\langle F(q)\rangle|^2$.

This factorization of $I(q)$ in form and structure factor according to eq 2 is valid for the spherical micelle and the vesicle phase in the limit of low polydispersity.[20,21]

The application of eq 1 for wormlike micelles is more questionable. To our knowledge, there is no simple (i.e. quasi analytical like Hayter−Penfold) structure factor for cylindrical charged objects.

The length of the cylindrical micelles being safely below the mean distance between them (cf. Appendix II), we argue that there is no entanglement of neighboring cylinders nor any angular correlation between them. The mean distance is then determined by the aggregation number and the concentration only, and at least the position of the first-order peak of the structure factor should be well-described by the structure factor of equivalent charged spheres of the same aggregation number. This procedure has been employed successfully by others,[22,23] and its validity has been shown by Monte Carlo simulations.[20b] There is an important approximation concerning the form factor of wormlike micelles: we know from cryo-TEM that these elongated micelles are flexible. Nevertheless, we can model them with spherical averaged rigid rods, as the exact form of the micelles does not have great effect on the spectra: the high-q part of the data for instance is sensitive to the cylindrical cross section only.

In any case, we do not include polydispersity in size in the data treatment, as charged micelles and vesicles are known to have pronounced energetic preference for a given aggregation number.[8b,24]

As a last point, we take into account the Gaussian distribution of wavelengths of the incident neutron beam around an average value $\lambda_m = 6.08$ Å:

$$G(\lambda,\lambda_m) = \frac{1}{\sqrt{2\pi}\Delta_\lambda}\exp\left(-\frac{(\lambda-\lambda_m)^2}{2\Delta_\lambda{}^2}\right) \qquad (3)$$

following the procedure given, for example, in ref 25. The wavelength spread $2\Delta_\lambda/\lambda_m$ on the order of 10% is due to the geometry of the mechanical wavelength selector. We suppose that this wavelength distribution dominates collimation effects and intensity smoothing related to the limited spatial resolution of the detector elements, which is true at least in the intermediate and high-q ranges.

In Figure 5 we have plotted the scattered intensity $I(q)$ for a sample without cosurfactant: Φ = 1.0%, Ω = 0.0, Γ = 3.55%. The correlation peak due to electrostatic interactions at q_o = 0.027 Å^{-1} is clearly visible, and the high-q part is dominated by the form factor. A fit of the form factor only confirms that the phase is a dilute dispersion of spherical micelles of average radius $R_s = 35 \pm 1$ Å. The full line in Figure 1 is the complete fit according to eq 2 taking into account the RMSA structure factor, the form factor given by eq A1 with $R_s = 35 \pm 1$ Å and the experimental smearing caused by the distribution of wavelengths, eq 3. The Debye length used in the structure factor has been calculated from the ionic concentration, which yields approximately 150 Å. The deviations at high wave vectors q between the measured and calculated intensity can be due to deviations from sphericity or monodispersity. The charge that is obtained as a result of the fitting procedure is $Q = 5 \pm 2$ elementary charges per micelle, which is less than that calculated from experimental parameters (Φ, Ω, Γ) and the radius (Q = 8). This discrepancy between the electrical charge of a micelle estimated from experimental parameters and the charge determined from the fit of the scattered intensity can have two reasons: it can first be due to a partial counterion condensation at the surface of the micelle. The dressed micelle model by Hayter[26a] applied to our data yields an adsorption of 30%, consistent with our measured charge. Second, it can stem from the use of the Yukawa potential or from the penetrating background (which we do not correct; see for example ref 26b) in the Hayter−Penfold procedure.

As one increases the relative amount of cosurfactant at fixed

concentration and charge, the spherical micelles grow and become rodlike. In Figure 6, we have plotted the scattered intensity for different cosurfactant-to-surfactant ratios $\Omega = 0.10$, $\Omega = 0.15$, and $\Omega = 0.20$ (at $\Phi = 1.0\%$, $\Gamma = 3.55\%$). The maximum of the intensity grows as the mean aggregation number grows, and the interaction peak shifts to lower q-values, as expected. The fit of only the form factor of an isotropically averaged infinite cylinder yields a radius of $R_c = 24 \pm 1$ Å. As an example, we plot the scattered intensity together with a complete fit according to eq 1 for $\Omega = 0.10$ in Figure 7. This fit is a combination of the RMSA structure factor, the spherical averaged form factors given by eqs A4 and A5 with $R_c = 23 \pm 1$ Å and the length $L = 200 \pm 5$ Å, and the experimental smearing caused by the distribution of wavelengths, eq 3. The charge obtained as a result of the fitting procedure is $Q = 12 \pm 2$ elementary charges per micelle, again less than the one expected from the experimental parameters only; compare the above comments.

Upon further increase of the cosurfactant-to-surfactant ratio Ω, the membrane becomes the thermodynamically stable aggregate. Because of the electric charges of the surface, the flat membrane is unstable with respect to curvature, and small unilamellar vesicles are formed. As there is no continuous topology conserving transformation from micelles to vesicles (i.e., it is impossible to continuously deform a micelle into a vesicle without cutting it in parts), we expect a shape transformation from a predominantly micellar to a predominantly vesicular population (coexisting without phase separation), as found by others.[27−29] This point is also confirmed by conductivity measurements presented below. The quantitative analysis of the scattered intensity of a mixture of micelles and vesicles of comparable sizes (within a factor of 2−3 in radius) in strong electrostatic interactions is very complicated and beyond the scope of this article. For example, the sample with $\Omega = 0.30$ (at $\Phi = 1.0\%$, $\Gamma = 3.55\%$) is clearly not interpretable in terms of only one morphology, whereas the spectrum of the sample with $\Omega = 0.35$ (at $\Phi = 1.0\%$, $\Gamma = 3.55\%$) is already well-describable in terms of only vesicles, although the fit is not completely satisfactory. In this case, the average radius of vesicles is 69 Å using the best fit.

At high cosurfactant-to-surfactant ratio finally, $\Omega > 0.35$, vesicles are the thermodynamically stable supramolecular aggregates. As an example, we plot the scattered intensity together with a complete fit for $\Omega = 0.60$ in Figure 8. It is again a combination according to eq 2 of the RMSA structure factor, the form factor given by eq A6 with $R_v = 70 \pm 5$ Å and a bilayer thickness of $\delta = 30$ Å, and the experimental smearing caused by the distribution of wavelengths, eq 3. The charge obtained is $Q = 32 \pm 2$ elementary charges per vesicle.

In Table 1 we sum up the SANS results on the transition. We report the observed aggregate geometry as a function of cosurfactant-to-surfactant ratio Ω. The transition from spherical micelles to wormlike micelles is found in the low-Ω range. We have characterized the following strong increase in length of the wormlike micelles with increasing Ω using a combination of the spherical averaged form factor and the RMSA structure factor. The micelle−vesicle coexistence region is localized between $\Omega = 0.25$ and $\Omega = 0.35$, and above $\Omega = 0.35$ monodisperse vesicles are found.

Conductivity. In this section we compare the conductivity of micellar and vesicular solutions. We observe a significantly lower conductivity in the vesicle phase ($\Omega = 0.60$) than in the micellar phase ($\Omega = 0.0$), as already observed by others, for example ref 30. Note that the concentration $\Phi = 1.0\%$ and relative amount of charges ($\Gamma = 4.0\%$) are fixed and identical, which indicates a change in the structure of the phase. In Figure 9, we monitor the evolution of the conductivity with the cosurfactant-to-surfactant ratio Ω. It is a rather smooth function of Ω, consistent with the picture of a phase transition between two types of populations—micelles and vesicles coexisting—with slowly changing relative proportions.

TABLE 1: Transition from Spherical Micelles to Wormlike Micelles to Vesicles as a Function of Cosurfactant-to-Surfactant Ratio Ω. R_s Is the Radius of the Spherical Micelle, R_c Is the Radius of the Cylindrical Micelle, R_v Is the Mean Vesicle Radius, and δ Is the Bilayer Thickness. R_s, R_c, and δ Are Deduced from the Form Factor; i.e., They Take a Possible Hydration into Account[a]

cosurfactant to surfactant ratio	morphology	geometry and charge number
$\Omega = 0.00$	spherical micelle	$R_s = 35 \pm 1$ Å $Q = 5 \pm 2$
$\Omega = 0.10$	wormlike micelle	$R_c = 23 \pm 1$ Å $L = 200 \pm 5$ Å $Q = 12 \pm 2$
$\Omega = 0.15$	wormlike micelle	$R_c = 24 \pm 1$ Å $L = 260 \pm 5$ Å $Q = 14 \pm 2$
$\Omega = 0.20$	wormlike micelle	$R_c = 24 \pm 1$ Å $L = 310 \pm 5$ Å $Q = 16 \pm 2$
$\Omega = 0.30$	wormlike micelles + vesicles	
$\Omega = 0.35$	wormlike micelles + predominantly vesicles	$R_v = 69 \pm 5$, $\delta = 33 \pm 1$ Å $Q = 32 \pm 2$
$\Omega = 0.40$	vesicle	$R_v = 67 \pm 5$, $\delta = 33 \pm 1$ Å $Q = 32 \pm 2$
$\Omega = 0.50$	vesicle	$R_v = 70 \pm 5$, $\delta = 33 \pm 1$ Å $Q = 32 \pm 2$
$\Omega = 0.60$	vesicle	$R_v = 70 \pm 5$, $\delta = 33 \pm 1$ Å $Q = 32 \pm 2$

[a] Spherical micelles−wormlike micelles−vesicles for a concentration of $\Phi = 1.0\%$ and a relative charge amount $\Gamma = 3.55\%$.

In Figure 10 we have reported the evolution of the conductivity with concentration Φ, for both the vesicular and the micellar phase. The difference in conductivity clearly increases with concentration, that of the vesicular phase being systematically below that of the micellar phase. At very low concentrations, $\Phi < 0.3\%$, the solutions have the same conductivity. We interpret this behavior as a transition from micelles to vesicles (at $\Omega = 0.60$) as the concentration increases: the vesicle population becomes more and more important. In addition to this, their mean size increases with Φ,[8b] thus further enhancing the difference in conductivity.

For a quantitative interpretation of the conductivity data, we will assume that the frequency (1000 Hz) of the measurement is sufficiently low to treat the problem in a static approximation. Furthermore, we will ignore the contribution of the supramolecular objects. In a first-order approximation, we will assume that the ions in the vesicles will not contribute to the conductivity of the solution. In ref 8b we have proposed a calculation of the proportion α of the ions inside the vesicles as a function of the experimental parameters. α is a function of the experimental parameters (Φ, Ω, Γ). This model is based on a numerical integration of the Poisson−Boltzmann equation for monovalent ions (negative counterions) within a Wigner−Seitz cell,[31,32]

$$\Delta\psi(\vec{r}) = \frac{en_-^o}{\epsilon\epsilon_o}\exp\left(\frac{e\psi(\vec{r})}{K_B T}\right) \tag{4}$$

where e is the charge of a proton, ϵ_o the vacuum electric

permittivity, ϵ the dielectric constant of water, Ψ the electric potential, K_B the Boltzmann constant, and n_-^o the counterion density at zero potential. We suppose that the ratio of the conductivity of the vesicular phase L_v and the micellar phase L_m is given by:

$$L_v/L_m = 1 - \alpha \quad (5)$$

In Figure 10, we confront this model with the experimental data: The full line is obtained by multiplying the measured conductivity of the micelles L_m by $(1 - \alpha)$. The theoretical curve passes between the two measured curves. The predicted difference in conductivity does not reproduce the experimental values, but it is correct in order of magnitude.

We propose a second, more elaborate model. It includes a possible adsorption of the conducting ions on the outside of the vesicles and micelles. Several methods for dealing with electrostatic adsorption within the framework of the Poisson−Boltzmann equation have been used in the past (cf. refs 26a, 33). We use the assumption that ions with electrostatic potentials higher than K_BT are adsorbed. After numerical integration of the Poisson−Boltzmann equation within a Wigner−Seitz cell it turns out that there is a higher proportion of ions adsorbed to a vesicle than to a micelle, thus further decreasing the conductivity of the vesicular solution with respect to the micellar one. In Figure 10, we plot the prediction of this model; that is, we multiply again the measured conductivity of the micelles L_m by a factor, which takes this time both the ions adsorbed outside the vesicles and the ions inside the vesicle into account. It clearly overestimates the difference in conductivity. Its deviation from the experimental curves at low volume fractions ($\Phi < 0.3\%$) is due to the assumption that there are only vesicles in solution for $\Omega = 0.60$ for all concentrations. We conclude that there is a partial adsorption of ions around supramolecular objects, which—with the effect of ions excluded from conductivity within the vesicles—explains experimental data at least qualitatively.

IV. Concluding Remarks

We have monitored the changes in aggregate morphology as a function of the cosurfactant-to-surfactant ratio and further elucidated the structure of the phase diagram of an amphiphilic system with strong electrostatic interactions. In contrast with the well-known evolution in neutral or screened systems (micelle−wormlike micelle−flat bilayer) described by the Israelachvili−Mitchell−Ninham theory and confirmed experimentally,[8a,17c] the micelle-to-vesicle transition here is triggered by electrostatics that destabilizes the flat bilayer (ref 8b and references therein). The modeling of the scattered intensities by a combination of the form and structure factor yields convincing results which are indeed supported by cryo-TEM micrographs. As far as the structure factor is concerned, it is well-known that the charge must be seen as a fitting parameter. However, it is interesting to note that—even if the charges are smaller than the ones calculated from the experimental parameters—charges are approximately proportional to the volume of the aggregate, for both spherical and wormlike micelles. The volume of the vesicles being approximately 10 times the volume of a spherical micelles, and taking into account that there is a certain number of counterions within the vesicle, this result is again consistent with the charge numbers determined for wormlike micelles and spherical micelles.

As far as the form factor is concerned, it is interesting to note that the micellar radii (of both cylindrical and spherical aggregates) are within 1 Å of the corresponding radii in the neutral system and are in line with cryo-TEM observation. A simple fit in terms of only the form factor even in the presence of electrostatic interactions yields correct radii (within 2 Å). Furthermore, for the cylindrical micelles, a fit according to eq 2 yields almost the same lengths and radii as the more complicated procedure according to eq 1. Using eq 1 amounts to neglecting the difference between $\langle|F(q)|^2\rangle$ and $|\langle F(q)\rangle|^2$. This does not have much influence on the fit, as the difference is negligible at low q where the structure factor dominates the intensity pattern, and at high q the structure factor is close to 1 and eq 1 reduces to eq 2. Nonetheless, a difference of a few percent between the curves generated with eqs 1 and 2 is visible. Finally, the length of the wormlike micelles measured by SANS is consistent with the result from cryo-TEM, which independently confirms our interpretation of the SANS spectra. We are thus able to quantitatively characterize the transition from micelles to vesicles. As far as the coexistence of vesicles and micelles is concerned, intermediate structures have been reported in the literature: open vesicles, mesh phases, or even patches and disks.[7b,34−36]

The transition from vesicles to micelles is also of importance in biological systems, for instance as a mechanism for therapeutic drug release. Extensive studies on the solubilization of monoalkyl amphiphile−cholesterol vesicles by detergents (octyl glucoside or TX-100) by cryo-TEM, dynamic light scattering, small-angle X-ray scattering, or turbidity measurements have been reported.[37] Qualitatively, these observations are similar to ours, as the starting point is a solution of weakly charged (5 wt % of dicetyl phosphate) unilamellar vesicles with a narrow size distribution around an average radius of $R = 350-400$ Å. Upon adding octyl glucoside, which has a relatively large nonionic headgroup, a transition to (generally globular) micelles is induced, just as by decreasing the cosurfactant-to-surfactant ratio in our system (i.e., increasing the TX-100 concentration).

The transition from vesicles to the lamellar phase has also aroused considerable interest in recent publications, especially in connection with the question of the existence of large multilamellar vesicles (or "onions") within the lamellar phase.[15−17,38] This idea is tempting as the curvature instability of flat membranes which is at the origin of vesicle formation could persist in the lamellar phase. It has already been shown by Boltenhagen et al. that close to the phase boundary onion-type defects are commonly observed.[39] We have evidence from static light scattering in the same system for the existence of onions in a limited region in the phase diagram close to the two-phase region separating the lamellar from the vesicular phase.[8a] We can now confirm from direct imaging (cryo-TEM) that we systematically find onions in the low concentration region ($\Phi = 0.05$) of the lamellar phase. In this study, the combination of imaging technique, namely, cryo-TEM, at the supramolecular level with scattering techniques is proven to be very helpful. Here, the model to be used is elucidated from a direct, model-independent technique from which qualitative structural information is obtained. The quantitative structural parameters are calculated from the scattering experiments.

Appendix I

The form factor of a homogeneous sphere of radius R_s and contrast $\Delta\rho$ is given by

$$\langle|F(q)|^2\rangle = |\langle F(q)\rangle|^2 = V_s^2\Delta\rho^2\left(3\frac{\sin(qR_s) - qR_s\cos(qR_s)}{(qR_s)^3}\right)^2 \quad (A1)$$

where V_s is the volume of the sphere.

The form factor of a homogeneous cylinder of radius R_c and full length L depends on the relative orientation to the scattering vector q, given by the angle γ between them. The Fourier transform of the contrast is given by

$$F(q) = 2V_L\Delta\rho \frac{J_1(qR_c \sin(\gamma))}{qR_c \sin(\gamma)} \frac{\sin\left(\frac{qL}{2}\cos(\gamma)\right)}{\frac{qL}{2}\cos(\gamma)} \quad \text{(A2)}$$

V_L is the volume of the cylinder and J_1 is the first-order Bessel function of the first kind. For the angles we have followed the convention of Penfold et al.[40] The angle γ between q and the cylinder axis is given by

$$\cos\gamma = \sin\Theta\cos\Psi\cos\Phi - \cos\Theta\sin\Psi \quad \text{(A3)}$$

where Θ is the polar angle of the cylinder axis, Φ is the azimuthal one, and Ψ is the angle between q and the x axis, if the detector is in the direction of the y axis.

As a cylinder is an anisotropic object, the orientational average of the square of $F(q)$ is not equal to the square of the orientational average. We thus write the averages separately:

$$\langle|F(q)|^2\rangle = \frac{1}{4\pi}\int\int_{\Theta=\pi,\,\Phi=2\pi}^{\Theta=0,\,\Phi=0}|F(q)|^2 \sin\Theta\, d\Theta\, d\Phi \quad \text{(A4)}$$

and

$$\langle F(q)\rangle = \frac{1}{4\pi}\int\int_{\Theta=\pi,\,\Phi=2\pi}^{\Theta=0,\,\Phi=0}F(q) \sin\Theta\, d\Theta\, d\Phi \quad \text{(A5)}$$

These integrals have been evaluated numerically.

Finally, the form factor of a homogeneous vesicle of inner radius R_i and outer radius R_o (or equivalently mean vesicle radius $R_v = (R_o + R_i)/2$ and bilayer thickness $\delta = R_o - R_i$) is given by

$$\langle|F(q)|^2\rangle = |\langle F(q)\rangle|^2 \frac{16\pi^2\Delta\rho^2}{q^6}[\sin(qR_i) - qR_i\cos(qR_i) - \sin(qR_o) + qR_o\cos(qR_o)]^2 \quad \text{(A6)}$$

Appendix II

The mean distance d between objects can be estimated by calculating the base of a (hypothetical) cubic Wigner−Seitz cell. Within the cell, the concentration (which is numerically close to the volume fraction) must equal the global concentration. For a cylinder of length L and radius R we obtain

$$\frac{V_{cyl}}{V_{cell}} = \frac{\pi R_c^2 L}{d^3} = \Phi \quad \text{(B1)}$$

The observed overlap of wormlike micelles in cryo-TEM gives a slightly misleading picture of average distances since the TEM micrographs gives a 2-D representation of a 3-D reality. Therefore, micelles at different depths in the sample are shown in the same plane. Moreover, the concave thin film of the sample[12] induces crowding of the aggregates.[18a]

References and Notes

(1) Hoffmann, H.; Thunig, C.; Schmiedel, P.; Munkert, U. *Langmuir* **1994**, *10*, 3982.

(2) (a) Brasher, L. L.; Herrington, K. L.; Kaler, E. W. *Langmuir* **1995**, *11*, 4267. (b) Kaler, E. W.; Herrington, K. L.; Murthy, A. K.; Zasadzinski, J. A. N. *J. Phys. Chem.* **1992**, *96*, 6698.

(3) Hervé, P.; Roux, D.; Bellocq, A. M.; Nallet, F.; Gulik-Krzywicki, T. *J. Phys. II Fr.* **1993**, *3*, 1255.

(4) Ristori, S.; Appell, J.; Porte, G. *Langmuir* **1996**, *12*, 686.

(5) Schomäcker, R.; Strey, R. *J. Phys. Chem.* **1994**, *98*, 3908.

(6) Radlinska E. Z.; Ninham, B. W.; Dalbiez, J. P.; Zemb, Th. *Coll. Surf.* **1990**, *46*, 213.

(7) (a) Regev, O.; Khan, A. *Progress Colloid Polym. Sci.* **1994**, *97*, 298. (b) Regev, O.; Kang, C; Khan, A. *J. Phys. Chem.* **1994**, *98*, 6619. (c) Regev, O.; Khan A. *J. Colloid Interface* **1996**, *182*, 95.

(8) (a) Oberdisse, J.; Couve, C.; Appell, J.; Berret, J. F.; Ligoure, C.; Porte, G. *Langmuir* **1996**, *12*, 1212. (b) Oberdisse, J.; Porte G. *Phys. Rev. E* **1997**, *56*, 1965.

(9) Bellare, J. R.; Davis, H. T.; Scriven, L. E.; Talmon, Y. *J. Electron. Microsc. Technol.* **1988**, *10*, 87.

(10) Vinson, P. K. In *The 45th Annual Meeting of the Electron Microscopy Society of America*; San Francisco Press, Inc.: San Francisco, 1987; p 644.

(11) Cabane, B. In *Surfactant Solutions: New Methods of Investigation*; Zana, R., Ed.; Marcel Dekker: New York, 1987.

(12) Harwigsson, I.; Söderman, O.; Regev, O. *Langmuir* **1994**, *10*, 4731.

(13) Süss, D.; Cohen, Y.; Talmon, Y. *Polymer* **1995**, *39*, 1809.

(14) Danino, D.; Talmon, Y.; Zana, R. *J. Colloid Interface Sci.* **1997**, *186*, 170.

(15) (a) Dubois, M.; Zemb, Th. *Langmuir* **1991**, *7*, 1352. (b) Dubois, M.; Gulik-Krzywicki, T.; Cabane, B. *Langmuir* **1993**, *9*, 673.

(16) Auguste, F.; Douliez, J. P.; Bellocq, A. M.; Dufourc, E. J. *Langmuir* **1997**, *13*, 666.

(17) (a) Thunig, C.; Platz, G.; Hoffmann, H. workshop on "Structure and Conformation of Amphiphilic Membranes", Jülich, 1991. (b) Hoffmann, H.; Munkert, U.; Thunig, C.; Valiente, M. *J. Colloid Interface Sci.* **1994**, *163*, 217. (c) Hoffmann, H.; Thunig, C.; Munkert, U.; Meyer, H. W.; Richter, W. *Langmuir* **1992**, *8*, 2629.

(18) (a) Talmon, Y. *Colloids Surf.* **1986**, *19*, 237. (b) Talmon, Y. *Ber. Bunsen-Ges. Phy. Chem.* **1996**, *100*, 364.

(19) (a) Hayter, J. B.; Penfold, J. *Mol. Phys.* **1981**, *42* (1), 109. (b) Hansen, J. P.; Hayter, J. B. *Mol. Phys.* **1982**, *46* (3), 651.

(20) (a) Klein, R.; D'Aguanno, B. in *Static Light Scattering: Principles and Developments*; Brown, W., Ed.; Oxford Press: 1996. (b) Weyerich, B.; D'Aguanno, B.; Canessa, E.; Klein, R. *Faraday Discuss. Chem. Soc.* **1990**, *90*, 245.

(21) Belloni, L. *J. Chem. Phys.* **1986**, *85* (1), 519.

(22) Pilsl, H.; Hoffmann, H.; Hofmann, S.; Kalus, J.; Kencono, A. W.; Lindner, P.; Ulbricht, W. *J. Phys. Chem.* **1993**, *97*, 2745.

(23) Quirion F.; Magid, L. *J. Phys. Chem.* **1986**, *90*, 5435.

(24) Mackintosh, F. C.; Safran, S. A.; Pincus, P. A. *Europhys. Lett.* **1990**, *12*, 697.

(25) McConnell, G. A.; Lin, M. Y.; Gast, A. P. *Macromolecules* **1995**, *28*, 20, 6754.

(26) (a) Hayter, J. B. *Langmuir* **1992**, *8*, 2873. (b) Snook, I. K.; Hayter, J. B. *Langmuir* **1992**, *8*, 2880.

(27) Pedersen J. S.; Egelhaaf, S. U.; Schurtenberger, P. *J. Phys. Chem.* **1995**, *99*, 1299.

(28) Khan A.; Marques E. In *Specialist Surfactants*; Robb, I. D., Ed.; Blackie Academic and Professional, Chapmann & Hall: New York, 1997.

(29) Oda, R.; Bourdieu, L.; Schmutz, M. *J. Phys. Chem. B* **1997**, *101*, 5913.

(30) Wuertz, J.; Hoffmann, H. *J. Colloid Interface Sci.* **1995**, *175*, 304.

(31) Marcus, R. A. *J. Chem. Phys.* **1955** , *23* (6), 1057.

(32) Alexander, S.; Chaikin, P. M.; Grant, P.; Morales, G. J.; Pincus, P.; Hone, D. *J. Chem. Phys.* **1994**, *80* (11), 5776.

(33) Belloni, L. In *Neutron, X-Ray and Light Scattering*; Lindner, P., Zemb, Th., Eds.; North-Holland, Delta Series: Amsterdam, 1991.

(34) Walter, A.; Vinson, P. K.; Kaplun, A.; Talmon, Y. *Biophys. J.* **1991**, *60*, 1315.

(35) Eduards, K.; Gustavsson, J.; Almgren, M.; Karlsson, G. *J. Colloid Interface Sci.* **1993**, *161*, 299.

(36) Marques, E.; Khan, A.; Miguel, M.; Lindman, B. *J. Phys. Chem.* **1993**, *97*, 4729.

(37) (a) Seras-Cansell, M.; Ollivon, M.; Lesieur, S., S. T. *P. Pharm. Sci.* **1996**, *6*, 12. (b) Seras, M.; Edwards, K.; Almgren, M.; Carlsson, G.; Ollivon, M.; Lesieur, S. *Langmuir* **1996**, *12*, 330. (c) Paternostre, M.; Meyer, O.; Grabielle-Madelmont, C.; Lesieur, S.; Ghanam, M.; Ollivon, M. *Biophys. J.* **1995**, *69*, 2476. (d) Vinson, P. K.; Talmon, Y.; Walter, A. *Biophys. J.* **1989**, *56*, 669.

(38) Radlinska, E. Z.; Zemb, T. N.; Dalbiez, J. P.; Ninham, B. W. *Langmuir* **1993**, *9*, 2844.

(39) Boltenhagen, P.; Kleman, M.; Lavrentovich *J. Phys. II* **1994**, 1439.

(40) Penfold, J.; Staples, E.; Cummins, P. G. *Adv. Colloid Interface Sci.* **1991**, *34*, 451−476.